Nonlinear stick-spiral model for predicting mechanical behavior of single-walled carbon nanotubes

Jingyan Geng and Tienchong Chang*
Shanghai Institute of Applied Mathematics and Mechanics, Shanghai University, Shanghai 200072, People's Republic of China
(Received 31 July 2006; revised manuscript received 31 October 2006; published 26 December 2006)

Based on a molecular mechanics concept, a nonlinear stick-spiral model is developed to investigate the mechanical behavior of single-walled carbon nanotubes (SWCNTs). The model is capable of predicting not only the initial elastic properties (e.g., Young's modulus) but also the stress-strain relations of a SWCNT under axial, radial, and torsion conditions. The elastic properties, ultimate stress, and failure strain under various loading conditions are discussed and special attention has been paid to the effects of the tube chirality and tube size. Some unique mechanical behaviors of chiral SWCNTs, such as axial strain-induced torsion, circumferential strain-induced torsion, and shear strain-induced extension are also studied. The predicted results from the present model are in good agreement with existing data, but very little computational cost is needed to yield them.

DOI: 10.1103/PhysRevB.74.245428 PACS number(s): 62.25.+g, 61.46.Fg

I. INTRODUCTION

The amazing mechanical properties such as exceptional high stiffness and tensile strength of carbon nanotubes (CNTs) make them highly potential and ideal candidates for multifarious applications including super-strong materials and nanomechanical devices.[1–3] Much efforts have been made to investigate the mechanical properties of CNTs because a clear understanding of these properties is essential to ensure the optimum performance of CNTs in potential applications.

There are many experimental studies that gave direct proof of the exceptional mechanical properties of CNTs. By investigating vibration frequencies of cantilevered CNTs within a transmission electron microscope (TEM), Treacy *et al.*[4] obtained the Young's modulus of multiwalled carbon nanotubes (MWCNTs) in the range from 0.4 to 4.15 TPa, with a mean value of 1.8 TPa; Krishnan *et al.*[5] found the Young's modulus of single-walled carbon nanotubes (SWCNTs) varying from 0.9 to 1.7 TPa;[5] Poncharal *et al.*[6] reported the Young's modulus of about 1 TPa for small diameter MWCNTs, while for the MWCNT with large diameters, the Young's modulus would be dramatically reduced up to 1 order because of the presence of rippling. By analyzing the bending behavior of MWCNTs which were manipulated by an atomic force microscope (AFM), Wong *et al.*[7] obtained an average value for the Young's modulus of 1.28 ± 0.59 TPa and Salvetat *et al.*[8] obtained a value of $0.81^{+0.41}_{-0.16}$ TPa, with no distinct dependence on the tube diameter. Yu *et al.*[9] directly applied axial tensile force on both ends of a MWCNT using two AFM tips, and measured the Young modulus ranging from 0.27 to 0.97 TPa and the ultimate strength of the outmost layer varying from 11 to 63 GPa. A unique failure mode of the MWCNT ("sword-in-sheath") was first observed in the work. Another direct measurement performed by Demczyk *et al.*[10] indicated that the ultimate strength of a MWCNT is about 150 GPa, and a value of 0.97 TPa derived for Young's modulus from a bending test was also reported.

Theoretical studies may provide more detailed information than an experimental investigation because a simultaneous measure of both mechanical behavior and structural details (such as the chirality) of a CNT remains a challenge to date. Two categories of theoretical approaches, namely the bottom-up approach based on quantum or molecular mechanics and the top-down approach based on continuum mechanics, are frequently used to study mechanical properties of nanostructured materials. Most of bottom-up approaches need a numerical procedure, such as molecular dynamics simulations, whereas many top-down methods are capable of giving analytical solutions to the problems considered.

Elastic properties and mechanical behavior of CNTs have been extensively studied by bottom-up calculations,[11–37] in which some studies paid special concerns on the effect of the structural details. Based on the Tersoff-Brenner potential, Robertson *et al.*[11] predicted by molecular dynamics that the elastic constants along the tube axis generally soften with decreasing tube radius. Similar results were reported in tight binding calculations by Hernandez *et al.*,[12] *ab initio* calculations by Sanchez-Portal *et al.*,[13] lattice dynamics calculations by Popov *et al.*[14] Some of these works showed that the elastic "constants" of a SWCNT are dependent on the tube chirality. The effects of geometrical detail on the failure[26–37] of a SWCNT have also been investigated. Two types of failure process, i.e., brittle fracture due to direct bond breaking and plastic deformation due to dislocation (Stone-Wales defect) evolution, were studied in these studies.[30–37] In particular, Nardelli *et al.*[31–34] showed by *ab initio* calculations that the mechanical behavior (including strain release mechanism and failure process) of nanotubes under large tensile strain strongly depends on their chirality and diameter. Extensive discussions on these dependences can also be found in a recent paper by Dumitrica *et al.*[37]

Bottom-up approaches may, in principle, be used to investigate the behavior of any systems if atomic interactions could be determined. However, direct simulation of large scale problems (with long time or large volume) remains a heavy computer task. To reduce computational costs, many top-down approaches[38–49] have been proposed to investigate the mechanical behavior of CNTs, which makes some large scale problems such as buckling of thick MWCNTs capable

of being studied. Besides, much effort has been made to derive explicit solutions based on continuum mechanics. For instance, following the pioneering work of Yakobson *et al.*,[15,30] thin shell theory was frequently use to analytically model CNTs.[50–58] The applicability and limitations of shell models was outlined in Wang *et al.*[59]

Recently, explicit solutions for the elastic properties of CNTs were derived within the framework of molecular mechanics, making the mechanical behavior of CNTs possible to be analytically investigated by bottom-up approaches. A truss model is presented by Odegard *et al.*[60,61] to establish the relation between effective bending rigidity and molecular properties of a graphene sheet by equating the molecular potential energy to the mechanical strain energy. A similar model was used by Wang[62] to obtain the effective in-plane stiffness and bending rigidity of achiral (i.e., armchair and zigzag) SWCNTs. Chang and Gao[63] established a "stick-spiral" model and obtained the first closed-form expressions for the longitudinal Young's modulus and Poisson's ratio of achiral SWCNTs. The closed-form expressions for elastic properties of achiral SWCNTs under various loading conditions were presented by Shen and Li[64] via a energy approach. Leung *et al.*[65] obtained Young's modulus for zigzag CNTs by developing an equivalent truss model. These expressions are concise but capable of directly linking material properties at different length scales. The effects of structural details on the elastic properties of CNTs can thus be reflected by these expressions. However, these results are limited to achiral nanotubes. The closed-form expressions for the axial elastic properties of chiral carbon nanotubes were presented more recently by Chang *et al.*[66,67] using the stick-spiral model. This model can also been used to investigate the effect of structural details on the buckling of CNTs.[68,69]

Despite many advantages such as high efficiency, the stick-spiral model currently suits only for studying mechanical behavior of chiral CNTs under small strains because in which harmonic potentials are used to model interatomic interactions. In a recent study, Belytschko *et al.*[26] provided a Morse type potential to describe the bond stretch and bond angle variation. The calculated results from this potential are in good agreement with those from Brenner's potential that is widely used to stimulate the mechanical behavior of CNTs. The potential may be readily introduced into the above analytical models to conduct an theoretical study of the mechanical behavior of chiral CNTs under large strains, as performed by Xiao *et al.*[70,71] for achiral tubes.

In this paper, we develop a nonlinear stick-spiral model by incorporating the Morse type potential presented by Belytschko *et al.*[26] into the fully established linear stick-spiral model.[67] The nonlinear mechanical behavior of chiral CNTs under large strains can thus be studied analytically. The model is shown to be highly efficient and accurate enough compared with the existing results. The effects of the tube size and tube chirality on the mechanical behavior of a SWCNT under axial loading, lateral pressure, and torsion are analyzed in detail. In particular, some unique mechanical behaviors of chiral SWCNTs, such as axial strain-induced torsion, circumferential strain-induced torsion, and shear strain-induced extension are also studied.

II. NONLINEAR STICK-SPIRAL MODEL OF A SWCNT

In the stick-spiral model,[63,66,67] an elastic stick with an axial stiffness of K_ρ and an infinite bending stiffness is used to model force-stretch relationship of the carbon-carbon bond, and a spiral spring with a stiffness of K_θ is used to model the twisting moment resulting from an angular distortion of the bond angle. In such a model, the total potential energy of a SWCNT can be given by

$$E = E_\rho + E_\theta = \frac{1}{2}\sum_i K_\rho (\mathrm{d}r_i)^2 + \frac{1}{2}\sum_j K_\theta (\mathrm{d}\theta_j)^2, \tag{1}$$

while the stretching force resulting from bond elongation and the twisting moment resulting from bond angle variation is calculated by

$$F^*(dr_i) = K_\rho dr_i, \tag{2}$$

$$M^*(\mathrm{d}\theta_j) = K_\theta \mathrm{d}\theta_j, \tag{3}$$

where dr_i is the bond elongation of bond i and $d\theta_j$ is the variance of bond angle j.

The above model is only suitable for analysis of mechanical behavior of CNTs under small deformations. When a SWCNT subjected to a relatively large strain is considered, nonlinear potentials must be introduced to describe the behavior of atoms far away from their equilibrium positions. In this paper, we choose a Morse type potential presented by Belytschco *et al.*[26] The total potential energy of a SWCNT is given by

$$E = E_\rho + E_\theta = \sum_i D_e\{[1 - \mathrm{e}^{-\beta(\Delta r_i)}]^2 - 1\} + \frac{1}{2}\sum_j k_\theta (\Delta\theta_j)^2[1 + k_{sextic}(\Delta\theta_j)^4], \tag{4}$$

with $D_e = 0.6031$ nN nm, $\beta = 26.25$ nm^{-1}, $k_\theta = 1.42$ nN nm/rad^2, $k_{sextic} = 0.754$ rad^{-4}, and Δ is the deference operator used to represents the variation of a parameter from its equilibrium value.The stretching force resulting from bond elongation and the twisting moment resulting from bond angle variation can be calculated by differentiating the first and the second terms of Eq. (4) with respect to bond elongation Δr_i and bond angle variation $\Delta\theta_j$, respectively

$$F^*(\Delta r_i) = 2\beta D_e(1 - \mathrm{e}^{-\beta\Delta r_i})\mathrm{e}^{-\beta\Delta r_i}, \tag{5}$$

$$M^*(\Delta\theta_j) = k_\theta \Delta\theta_j[1 + 3k_{sextic}(\Delta\theta_j)^4]. \tag{6}$$

Once Eqs. (2) and (3) are replaced by Eqs. (5) and (6) in a original stick-spiral model, a nonlinear model can be established straightforwardly. More details are shown in Appendix A. The definitions of some physical parameters to be discussed, such as stress and strain, can be found in Appendix B.

III. RESULTS AND DISCUSSIONS

A. Axial loading

The nonlinear stress-strain relationships are shown in Fig. 1 for axial loaded SWCNTs with different chiralities. It is

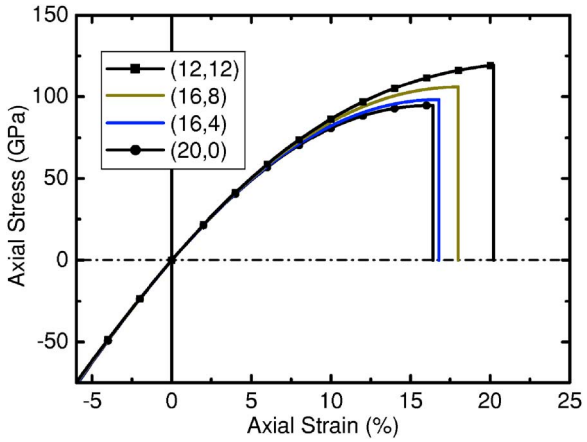

FIG. 1. (Color online) Chirality dependent axial stress-strain relationships for SWCNTs.

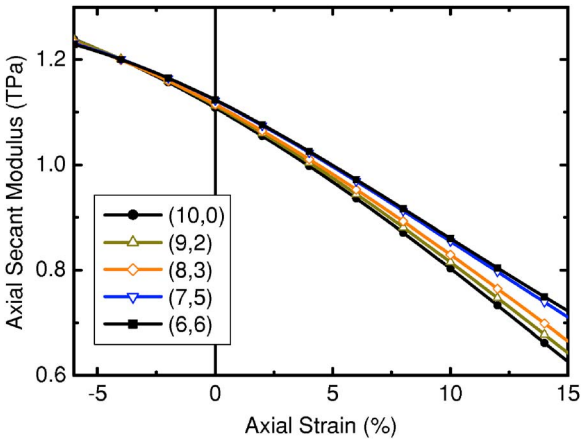

FIG. 3. (Color online) Dependence of the axial secant modulus on the axial strain.

seen that the linear response of a SWCNT is confined within a very small strain region ($\sim \pm 3\%$). With increasing tensile strain, the stress-strain curve tends to flatten out, indicating that the SWCNT under tension is strain softening. In contrast to the tensile case, the SWCNT under compression is strain hardening. The tensile stress-strain relations from the present analytical approach agree well with those from the numerical simulations based on molecular dynamics[29,35,36] and molecular mechanics.[26] In the present paper, we focus only on the bond breaking failure mode and the calculations under axial compression are terminated at a relatively small strain (that is assumed not beyond the buckling threshold). The procedure of investigating the CNT buckling using the stick-spiral model can be seen in our previous works.[68,69]

Figure 2 shows the initial axial Young's modulus against the tube diameter. Here the initial modulus is defined as the slope of the stress-strain curve at zero strain. We see that the initial Young's modulus increases with increasing tube diameter, approaching a limit value of graphite. For a given tube diameter, the initial Young's modulus increases with increasing tube chiral angle. The smaller the tube diameter, the stronger the dependence of the Young's modulus on the tube size and tube chirality. The effects of tube chirality and tube

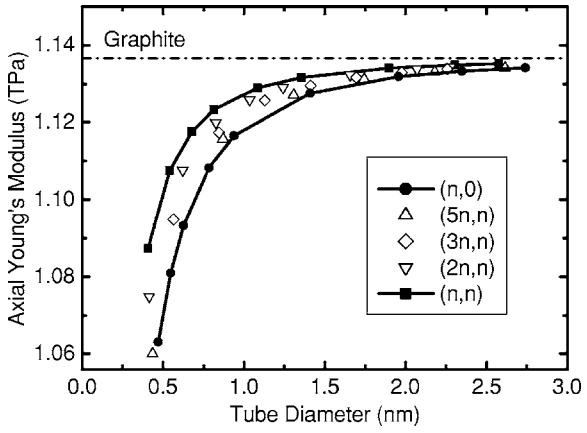

FIG. 2. Chirality and size dependent initial axial Young's modulus of SWCNTs.

size may be neglected when the tube diameter is larger than 2.0 nm. The present predictions for the initial Young's modulus are in reasonable agreement with those given by various theoretical methods. Many works such as tight bonding calculations,[12] lattice dynamics,[14] and atomistic-based continuum analysis[43] showed that Young's modulus increases with increasing tube diameter. Tight binding simulations by Hernandez *et al.*[12] gave the values for the Young's modulus ranging from 0.91 TPa to 1.25 TPa. *Ab initio* calculations by Sanchez-Portal *et al.*[13] showed that the Young's modulus varies from 0.97 to 1.09 TPa. The present results agree well also with existing experimental data for Young's modulus of CNTs. Using an atomic force microscopy, Wong *et al.*[7] measured a Young's modulus of 1.28 ± 0.59 TPa; Salvetat *et al.*[8] obtained an average Young's modulus of 1 TPa. Similar results were reported by Krishman *et al.*[5] using a transmission electron microscope ($1.3^{+0.6}_{-0.4}$ TPa) and Yu *et al.*[9] using a scanning electron microscope (~ 1 TPa). The Young's modulus of graphite can be obtained as 1.14 TPa (corresponding to an in-plane stiffness of 386 J/m^2) by the limiting case of a SWCNT with an infinite diameter, in good agreement with experimental value of 1.06 TPa.

It should be noted that different definitions of effective tube thickness would result in different values of Young's modulus of a SWCNT. For example, with the effective tube thickness varying from 0.066 nm to 0.69 nm reported in the literatures, the difference between the maximum and the minimum value of the calculated Young's moduli will be more than 10 times. However, when the surface Young's modulus (or the in-plane stiffness) is used, the deviation resulted from ill-defined tube thickness will be eliminated.[63] We note further that Young's modulus may also be defined using the whole cross section (the SWCNT is viewed as a solid cylinder) rather than the net cross section (the SWCNT is viewed as a hollow cylinder, as in this paper). The calculated Young's modulus following this definition will decrease with increasing tube diameter.[64]

Figure 3 shows the secant axial modulus versus axial strain for SWCNTs with different chiral angles but approximately the same diameter. We see that the axial elastic modulus shows strong dependence on the axial strain. With in-

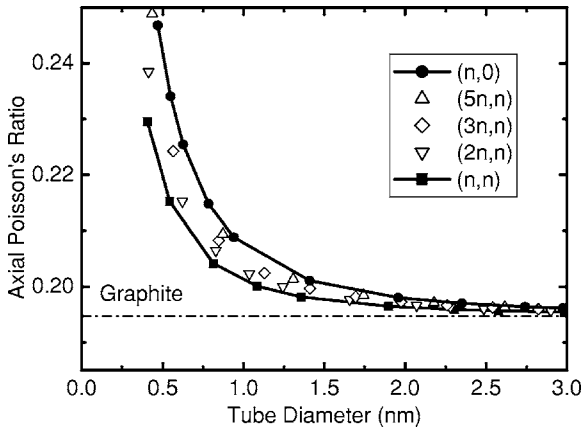

FIG. 4. Chirality and size dependent axial Poisson's ratio of SWCNTs.

creasing tensile strain, the secant modulus of a SWCNT decreases almost in a linear fashion. The secant modulus depends also on the tube chirality, especially at large strains. For instance, the maximum deviation of the secant modulus due to different chirality may be more than 10% when the tensile strain is larger than 10%, even for large tubes.

Longitudinal Poisson's ratio as a function of the tube diameter is shown in Fig. 4. Poisson's ratio decreases with increasing tube diameter, approaching the limit value (0.195) of graphite for large tubes. For a given tube diameter, Poisson's ratio decreases with an increasing in tube chiral angle. The chirality and size dependence is significant only for the tubes with diameters smaller than 2.0 nm. Although the present results are in reasonable agreement with some existing data (e.g., Sanchez-Portal *et al.*[13]), there is no unique opinion that is widely accepted for the dependence of Poisson's ratio on the tube diameter. Even completely contrary conclusions were reported in the literatures. Tight binding calculations by Hernandez *et al.*[12] indicated that Poisson's ratio for armchair tubes increases from 0.247 to 0.256 with increasing tube diameter from (6,6) to (15,15), while for zigzag tubes, Poisson's ratio decreases from 0.275 to 0.270 with increasing tube size from (10,0) to (20,0). To the contrary, Popov *et al.*[14] obtained that, with increasing tube diameter, Poisson's ratio decreases for armchair tubes, but increases for zigzag tubes. The contradiction may be attributed to two aspects. First, there is no sufficient data to eliminate the possible calculating errors during numerical procedures. For instance, only two points are available for zigzag tubes in Hernandez *et al.*'s work. Second, the relationship between Young's modulus and shear modulus from continuum mechanics is frequently used to extract Poisson's ratio from numerical data, as in Popov *et al.*'s work. In fact, recent findings from both molecular dynamics calculations[21] and analytical investigations[67] showed that this relationship is not retained for a SWCNT. Hence if the formula from isotropic continuum mechanics was directly used to calculate Poisson's ratio, severe deviations must be caused. Despite the mentioned contrary results, as can be expected, the present results show the same trends as all the previous calculations based on molecular mechanics approach.[63,64,66,67,70]

Many efforts have been made to investigate the failure of SWCNTs under axial tension, and two primary failure processes were observed in the studies.[30–37] The first one is brittle fracture (via direct bond breaking), while the second is plastic deformation (via Stone-Wales bond rotation). Brittle failure always leads to a sudden fracture of SWCNTs, whereas plastic deformation may result in necking phenomenon through dislocation evolution.[31,35] Brittle-to-ductile transition has been extensively discussed by Nardelli *et al.*[31,32] and Dumitrica *et al.*[37] from an atomic point of view. They found that the failure mode of a SWCNT depends not only on tube chirality, but also on applied strain rate and ambient temperature.[31–34,37] It is obvious that the present simple analytical model could not capture both the two modes because bond rotation behavior is not taken into account. Thus it predicts only bond breaking (brittle) failure. That is, once the tube failed (corresponding to the inflection point of a local broken bond), its loading capacity losses immediately.[71] This is the favorable failure mode at low temperatures. On the other hand, the present model is based on an empirical potential[26] that may not be very accurate under very large strains compared to quantum mechanical calculations, as discussed extensively by Zhao *et al.*[34] Hence, the present model gives only reference values for tensile strength and failure strain of SWCNTs under brittle fracture, and more accurate results should be obtained by experiments,[9,10] molecular dynamics, or *ab initio* calculations.[26–37]

The ideal tensile strength of the SWCNT under brittle fracture is the maximum value of the tensile stress which is approached at the inflection point of the stress-strain curve.[26,27,70,71] The failure strain is the applied strain corresponding to the tensile strength. Shown in Figs. 5(a) and 5(b) is respectively the axial tensile strength and failure strain versus tube diameter. Significant influence of the tube chirality on the tensile strength and failure strain can be seen in the figure. Of particular interest is that the tensile strength is insensitive to the tube diameter, and so does the failure strain. Both the tensile strength and failure strain approach their limit values when the tube diameter is larger than 1 nm. The tensile strength and the failure strain for armchair tubes (120 GPa and 21%) are about 25% and 30% higher than those for zigzag tubes (95 GPa and 16.4%), respectively. Our predictions are in reasonable agreement with some existing results. Molecular mechanics simulations by Belytschko *et al.*[26] predicted that the tensile strengths and failure strains of armchair and zigzag tubes are 112 GPa and 18.7%, and 93.5 GPa and 16%, respectively. They found also that the tube size has no effect on the tensile strength. Ogata and Shibutani[27] using a tight binding method gave the tensile strength of about 108 GPa and 114 GPa for zigzag and armchair SWCNTs, respectively. Molecular dynamics simulations by Xiao *et al.*[29] indicated that the tensile strengths for both armchair and zigzag SWCNTs are about 80 GPa, while the failure strain for zigzag and armchair tubes are 15% and 17%, respectively. Liew *et al.*[35] obtained by molecular dynamics a tensile strength of 114 GPa and a failure strain of 28% for (10, 10) tubes.

The axial tensile strength and failure strain of SWCNTs (with diameters larger than 2 nm) versus the tube chirality is shown in Fig. 6. It is seen that, with increasing tube chiral angle, the tensile strength of a SWCNT increases monotonously. However, the variation of the axial failure strain is

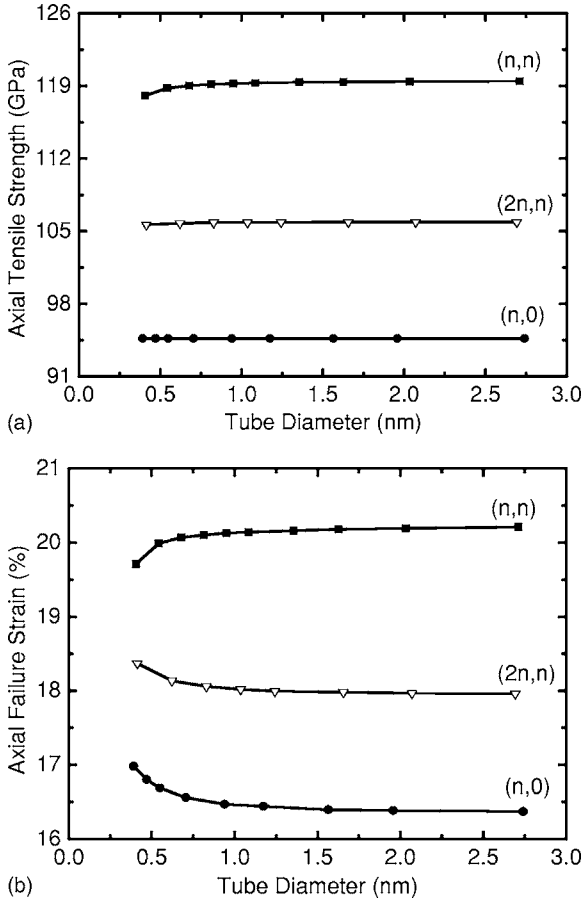

FIG. 5. (a) Axial tensile strength versus tube diameter. (b) Axial failure strain versus tube diameter.

quite complicated. With an increase in the chiral angle, the failure strain increases first to its maximum value at a chiral angle of about 26°, then decreases to a local minimum at about 29°, and then increases to the value for armchair tubes. The full curve for the failure strain is just like a long dipper. To reveal the physics behind the curve, further study is needed. Results from molecular mechanics simulations by

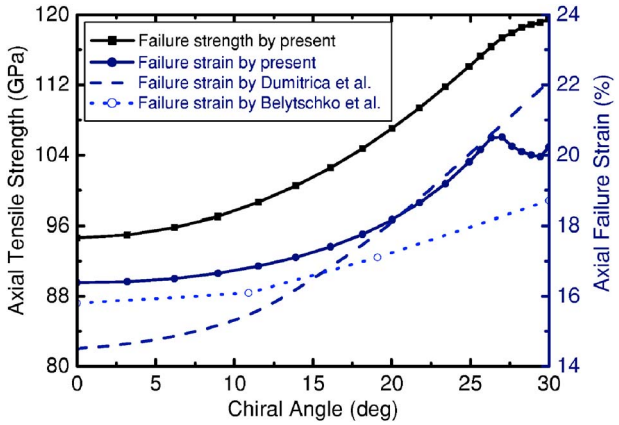

FIG. 6. (Color online) Variation of axial tensile strength and failure strain against tube chiral angle. Note that although the tensile strength is increases with increasing chiral angle, the variation of failure strain is not monotonic.

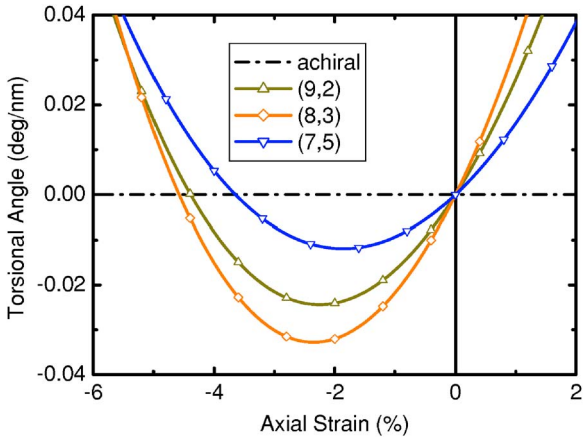

FIG. 7. (Color online) Axial strain-induced torsion angle of chiral SWCNTs with approximately the same diameter. The maximum untwisting angle occurs for SWCNTs with a chiral angle of about $\pi/12$. Note that a chiral SWCNT will twist in the same direction under a relatively large compressive strain and under a tensile strain.

Belytschko *et al.*[26] and quantum mechanics based calculations by Dumitrica *et al.*[37] are also presented for comparison and reasonable agreements are found. We note that the present predicted ideal tensile strength and the failure strain, as well as the mentioned theoretical results, is significantly higher than some experimental values. For example, Yu *et al.*[9] measured the tensile strength ranging from 11 to 63 GPa, and the failure strain from 10% to 13% using a scanning electron microscope; Walters *et al.*[72] using atomic force microscopy obtained the tensile strength of 45±7 GPa for SWCNTs. The lower experimental values might be attributed to the presence of defects, the measuring errors, and so on.

We investigated also a very interesting phenomenon of so-called axial strain-induced torsion (ASIT). Due to the geometrical asymmetry, torsional deformation may occur even in a chiral SWCNT subjected only to an axial loading. It is seen from Fig. 7 that the ASIT angle increases monotonously with an increasing in tensile strain. Namely, a chiral SWCNT is twisted by an axial tensile strain. However, the ASIT of a SWCNT under compression is quite different. With increasing compressive strain, the induced torsional angle decreases under a relatively small strain, but increases after the strain is larger than a critical value. In other words, when subjected to an axial compressive strain, a SWCNT untwists first and then twists again. This means that a relatively large compressive stain and a tensile strain will twist a chiral SWCNT in the same direction. It is very likely that ASIT would modify the electric properties of an axial loaded SWCNT. Hence this feature should be paid special attention in designing CNT-based electromechanical devices in which high sensitivity must be ensured. Figure 7 shows also that the ASIT of a chiral SWCNT is significantly dependent on the tube chirality. For a given tube diameter, the maximum untwisting angle induced by axial compressive strain increases with increasing tube chiral angle for tubes with chiral angle smaller than $\pi/12$, while for tubes with chiral angle larger than $\pi/12$, the maximum untwisting angle decreases with

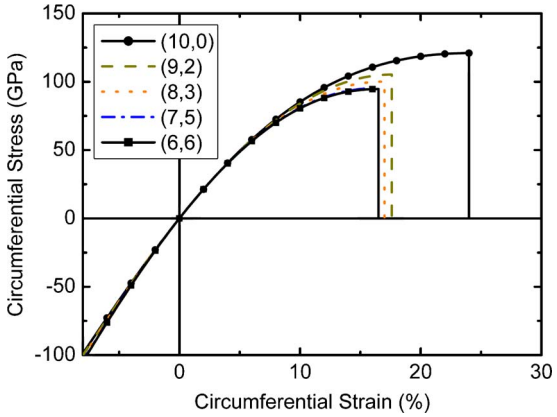

FIG. 8. (Color online) Chirality dependent circumferetial stress-strain relationships for SWCNTs.

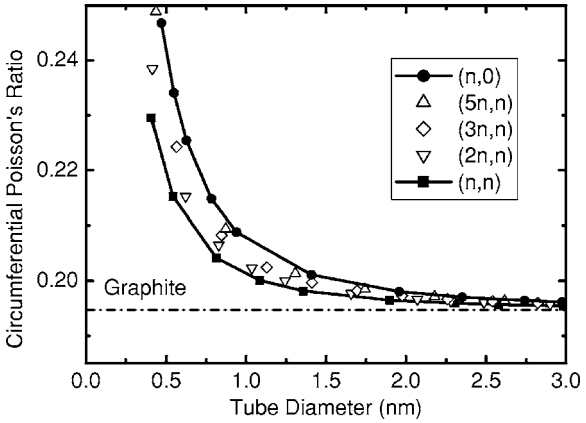

FIG. 10. Chirality and size dependent circumferential Poisson's ratio of SWCNTs.

increasing tube chiral angle. These observations consist very well with those given by a two-dimensional continuum model[18] and those from molecular dynamics simulations.[24]

B. Radial pressure

Figure 8 shows the nonlinear stress-strain relationships under radial pressure for different SWCNTs with approximately the same diameters. Very similar to the case of axial loading, a SWCNT may be softened by an internal pressure, but hardened by an external pressure.

The initial circumferential Young's modulus and Poisson's ratio versus tube diameter are shown respectively in Figs. 9 and 10. It is interesting to find that the circumferential elastic modulus and Poisson's ratio of a SWCNT exactly equal to those along axial direction, in agreement with our previous observations.[67] However, it should be noted that the elastic properties of a SWCNT are strongly strain dependent due to their significant nonlinearity, which consequently leads to a unique elastic anisotropy of SWCNTs, i.e., strain-induced elastic anisotropy (SIEA).

Figure 11 shows the secant circumferential modulus as a function of circumferential strain. We can see that the secant modulus almost linearly decreases with increasing circumferential strain. The larger the chiral angle, the higher the decreasing rate. As a result, the secant circumferential modulus of a SWCNT at large circumferential tensile strain (say $>3\%$) will reverse their dependence to the tube chirality, i.e., decreases with increasing tube chiral angle, in contrast to the initial circumferential modulus (see Fig. 9). Namely, the secant circumferential modulus of an armchair SWCNT will be smaller than a zigzag SWCNT under a relatively large circumferential tensile strain. Our results show also that the secant modulus under large strain (say $>5\%$) depends more significantly on tube chirality.

The circumferential tensile strength and the failure strain are presented in Figs. 12(a) and 12(b), respectively. In contrast to the axial tensile case, a SWCNT having the smaller chiral angle possesses a larger circumferential tensile strength and failure strain. For instance, the circumferential tensile strength and failure strain for zigzag nanotubes (121 GPa and 23%) are, respectively, about 25% and 50% higher than those for armchair nanotubes (95 GPa and 16%). As can be expected, due to the geometrical similarity along tensile direction in graphene plane, the circumferential tensile strength and failure strain for zigzag (or armchair) tubes are very close to the longitudinal tensile strength and failure strain for armchair (or zigzag) tubes. We see also from the

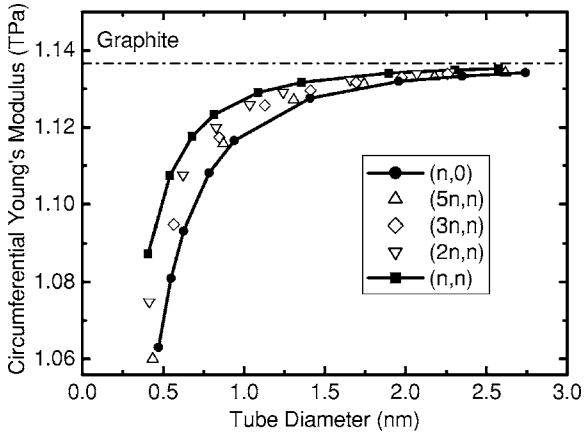

FIG. 9. Chirality and size dependent initial circumferential Young's modulus of SWCNTs.

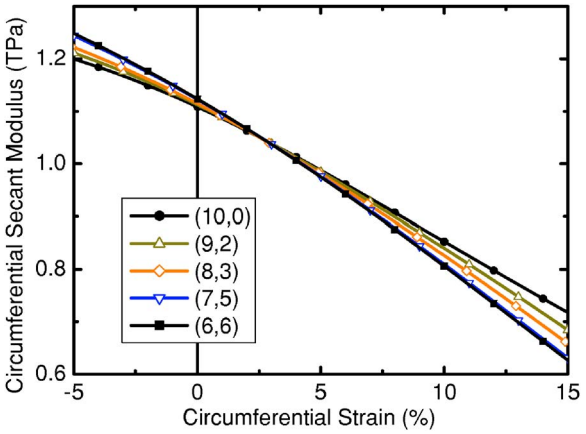

FIG. 11. (Color online) Dependence of the circumferential secant modulus on the circumferential strain.

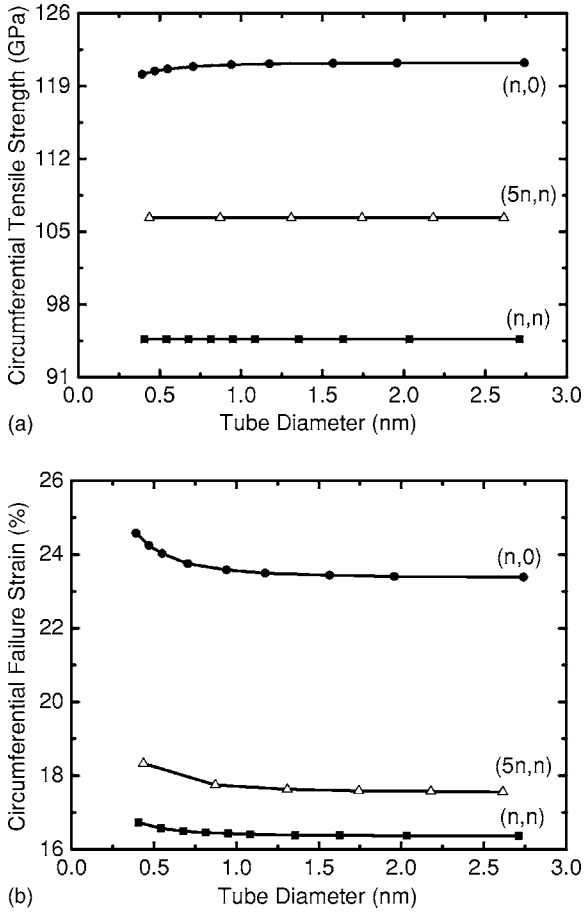

FIG. 12. (a) Circumferential tensile strength versus tube diameter. (b) Circumferential failure strain versus tube diameter.

two figures that both the circumferential tensile strength and failure strain are insensitive to the tube diameter. Figure 13 shows the circumferential tensile strength and failure strain versus tube chirality for SWCNTs with diameters larger than 2 nm. We can see that both the tensile strength and failure strain decrease monotonously with increasing chiral angle.

Similar to the case of axial loading, torsion deformations may also be induced by the circumferential strain (see Fig. 14). In contrast to ASIT, the circumferential strain-induced

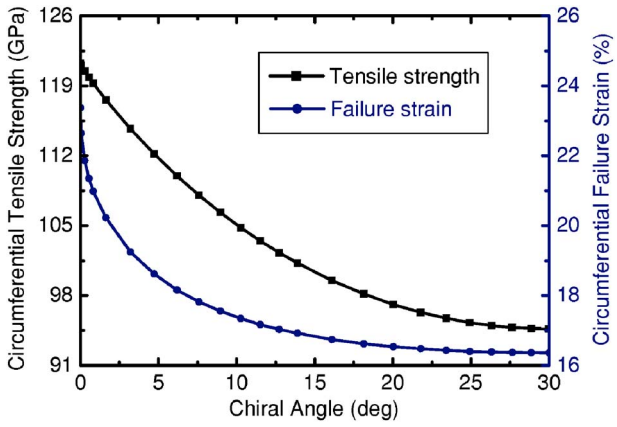

FIG. 13. (Color online) Circumferential tensile strength and failure strain versus tube chirality.

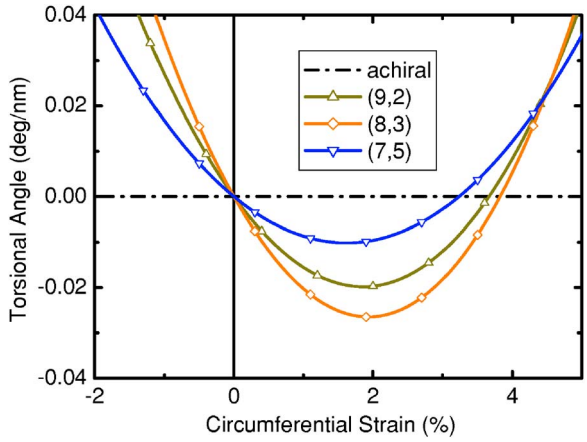

FIG. 14. (Color online) Circumferential strain-induced torsion angle of chiral SWCNTs with approximately the same diameter. The maximum untwisting angle occurs for SWCNTs with a chiral angle of about $\pi/12$. Note that a relatively large tensile strain will result in a torsion in the same direction as under a compressive strain.

torsion (CSIT) angle of a SWCNT under compressive circumferential strain (external pressure) increases monotonously with increasing strain, while under tensile circumferential strain (internal pressure), with increasing strain, the torsional angle decreases under a relatively small strain, but increases once the strain beyond a critical value. This means that, when subjected to an internal pressure, a SWCNT untwists first and then twists again in the opposite direction, i.e., the same sense as under external pressure. We see from Fig. 14 that the tube chirality has significant effect on the CSIT of a SWCNT. The maximum untwisting angle occurs for tubes with a chiral angle of $\pi/12$, and vanishes for achiral tubes.

C. Torsion loading

Figure 15 shows stress-strain relationships under torsion for SWCNTs with different chiral angles. The torsional re-

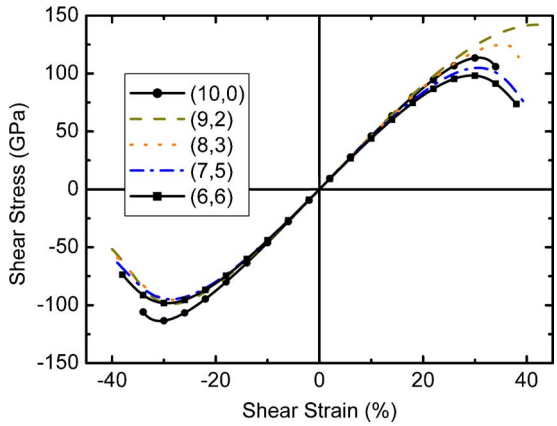

FIG. 15. (Color online) Shear stress-strain curves for SWCNTs with different chiralities. Note that the torsion response of a chiral SWCNT is significantly dependent on the twisting direction because of their geometrical asymmetry.

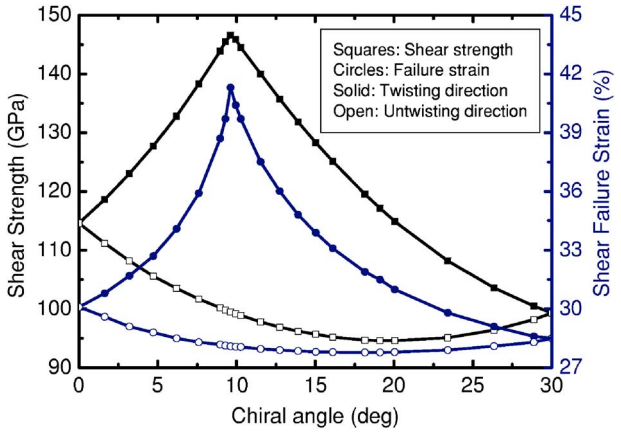

FIG. 16. (Color online) Non-monotonous variations of ideal shear strength and failure strain versus tube chiralty. Note that the shear strength and failure strain of a chiral SWCNT in the twisting and untwisting directions are quite different.

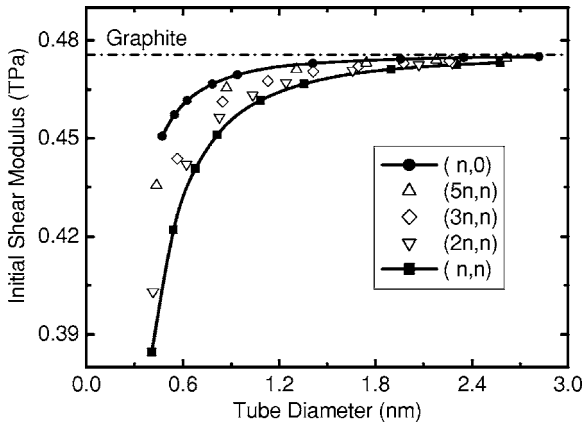

FIG. 17. Chirality and size dependent initial shear modulus of SWCNTs.

sponse of a SWCNT is in fact more complicated than the above two cases, because the failure mode of a SWCNT under torsion might be either fracture or buckling, depending on tube size as well as constraint exerted on the tube. Hence we simply define the shear stress and strain at the inflection point of the stress-strain curve as the ideal shear strength and failure strain. We believe such definitions would give reference values for the upper limits of the shear strength and failure strain of a SWCNT. Figure 15 shows that the torsion response of a SWCNT is almost linear in a relatively large strain range (±10%), which agrees well with the findings for zigzag tubes from a molecular dynamics simulation by Yakobson *et al.*,[15] and from an *ab initio* calculation by Ertekin and Chrzan.[73] A very important phenomenon to which special attention should be paid is that the mechanical behavior of a chiral SWCNT is dependent on the torsion direction, which could be seen more clearly in the following discussions.

The dependences of the ideal shear strength and failure strain on the tube chirality are shown in Fig. 16 for SWCNTs with diameters larger than 2 nm. To our surprise, we find that the variations of both the two mechanical properties are not monotonic. In twisting direction, with increasing chiral angle from zero to $\pi/6$, the ideal shear strength and failure strain increase from the values (115 GPa and 30.1%) for zigzag tubes to their maximum values (146 GPa and 41.3%) at a chiral angle of about $\pi/18$ (9.6 degree in our calculations, slightly dependent on tube diameters), and then decreases to the values (99 GPa and 28.5%) for armchair tubes. In untwisting direction, however, with increasing chiral angle from zero to $\pi/6$, the ideal shear strength and failure strain decrease from the values (115 GPa and 30.1%) for zigzag tubes to their minimum values (95 GPa and 27.8%) at a chiral angle of about $\pi/9$ (18.1° in our calculations, slightly dependent on tube diameters), and then increases to the values (99 GPa and 28.5%) for armchair tubes. The curves for the shear strength along both the twisting and untwisting directions form a sail-like pattern, so does the curves of the shear failure strain. It is found that the ideal shear strength and failure strain for achiral tubes are independent of the loading directions due to their geometrical symmetry, and both the mechanical properties for zigzag tubes are slightly higher than those for armchair tubes.

The initial shear modulus as a function of tube diameter is shown in Fig. 17. We can see that the initial shear modulus increases with increasing tube diameter and approaches the predicted graphite value. For a given tube diameter, a nanotube with a smaller chiral angle has a larger initial shear modulus. When the tube diameter is larger than 2 nm, the dependences of the initial shear modulus on the tube chirality and tube size are ignorable. The present results are in good agreement with some existing predictions, such as those from lattice dynamics by Popov *et al.*,[14] molecular dynamics simulations by Wang *et al.*[21] and Gupta *et al.*,[74] molecular mechanics calculations by Xiao *et al.*[70] When the tube diameter approaching infinite, the shear modulus of graphite can be predicted as 0.48 TPa, in good agreement with the experiment value of 0.44±0.03 TPa.

Figure 18 presents the secant shear modulus against shear strain. It is seen that the secant shear modulus of a SWCNT slightly dependent on the shear strain. With a variation of the shear strain from −10% to 10%, the maximum deviation of the secant shear modulus of a SWCNT is no more than 5%. This confirms the observation in Fig. 16 that the torsion be-

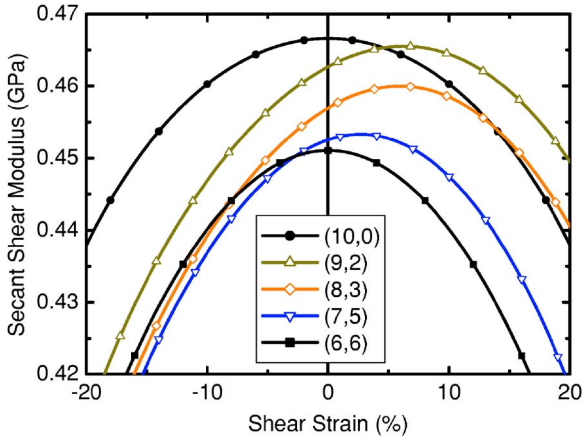

FIG. 18. (Color online) Dependence of the secant shear modulus on the shear strain.

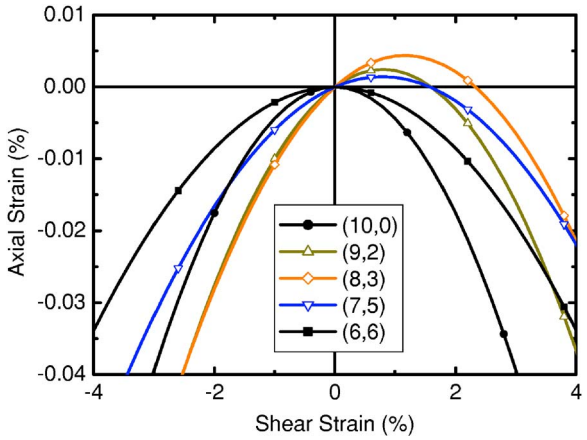

FIG. 19. (Color online) Shear strain-induced axial extension of chiral SWCNTs with approximately the same diameter. Note that a chiral SWCNT can even be elongated by a torsion in the twisting direction.

havior of a SWCNT is almost linear in a relatively large strain range. We see also that the secant shear moduli for achiral SWCNTs decrease with increasing shear strain, and are independent of the torsional direction, as can be expected according to their geometrical symmetry. However, the secant shear moduli for chiral SWCNTs show dependence on the torsional directions. The secant shear moduli of a chiral SWCNT decreases monotonously with increasing shear strain along the untwisting direction, while with increasing shear strain along the twisting direction, the secant shear moduli increase first and then decrease once the shear strain beyond a critical value. This critical value is dependent on the tube chiral angle. Our results indicate that the largest critical shear strain is approached at a chiral angle of about $\pi/12$.

We have discussed axial strain induced-torsion and circumferential strain induced torsion in the above sections. A natural question now is whether a shear strain could induce an axial extension in a chiral SWCNT? The answer can be found in Fig. 19 where the variation of the shear strain-induced extension (SSIE) is presented. It is seen that a chiral SWCNT is shortened monotonously with increasing shear strain along the tube twisting direction. However, with increasing shear strain along the tube untwisting direction, the SWCNT is slightly elongated first and then is shortened after the shear strain beyond a critical value. The maximum elongation occurs in the SWCNT with a chiral angle of $\pi/12$. No matter in which direction an achiral SWCNT is twisted, it is always shortened. It is found also that the SSIE of a zigzag tube is more remarkable than that of an armchair tube with the same diameter.

IV. CONCLUDING REMARKS

A nonlinear stick-spiral model is developed based on a molecular mechanics concept. The model presents a simple analytical method to investigate the nonlinear mechanical behavior of chiral SWCNTs under large strains. Comparisons with existing results show that the present model is highly efficient and capable of giving reasonable predictions for mechanical properties of SWCNTs.

The mechanical behavior of a SWCNT shows significant nonlinearity under axial loading and lateral pressure. The elastic modulus of a SWCNT is strongly dependent on the corresponding strain. With increasing tensile train, the corresponding secant modulus decreases approximately in a linear fashion. Although the effects of tube size and tube chirality on the initial elastic properties are remarkable only for SWCNTs with diameter smaller than 2 nm, the secant modulus under large strain is significantly influenced by tube chirality even for large tubes. In contrast, the torsion response of a SWCNT is almost linear in a relatively large strain range. Of particular interest is that the torsion behavior of a chiral SWCNT is dependent on the loading directions because of their geometrical asymmetry.

The tensile strength and failure strain of a SWCNT are significantly dependent on the tube chirality, but insensitive to the tube diameter. With increasing tube chiral angle, the axial tensile strength increases from 95 GPa for zigzag tubes to 120 GPa for armchair tubes, while the circumferential tensile strength decreases from 121 GPa to 95 GPa. Although the circumferential failure strain decreases monotonously with increasing chiral angle, the curve for the axial failure strain is quite complicated and shows a dipperlike shape. The ideal shear strength and failure strain depend not only on the tube chirality, but also on the loading direction. With increasing tube chiral angle from 0 to $\pi/6$, they increase from the values (115 GPa and 30%) for zigzag tubes to their maximum values (146 GPa and 41%) at a chiral angle of $\pi/18$ in the twisting direction but decrease to their minimum values (95 GPa and 27.8%) at a chiral angle of $\pi/9$ in the untwisting direction, and then approach the values (99 GPa and 28.5%) for armchair tubes. The curves for both the shear strength and failure strain along twisting and untwisting directions form an interesting sail-like pattern.

Some unique mechanical behaviors of a chiral SWCNT, such as axial strain-induced torsion, circumferential strain-induced torsion, and shear strain-induced extension are studied. The results show that torsion deformation is always coupled with both axial and circumferential deformations in a chiral SWCNT due to the geometrical asymmetry. Special attentions in future should be paid for nonmonotonous coupling of torsion deformation with axial and circumferential deformations, which may brings new insights in understanding the coupling effects on some carbon nanotube based electromechanical devices.

ACKNOWLEDGMENTS

We gratefully acknowledge the financial support from the National Natural Science Foundation of China (Contract No. 10402019), Shanghai Rising-Star Program (05QMX1421), and Shanghai Leading Academic Discipline Project (Y0103).

APPENDIX A

A SWCNT can be viewed as a graphene sheet rolled into a seamless tube with a diameter on the order of nanometers.

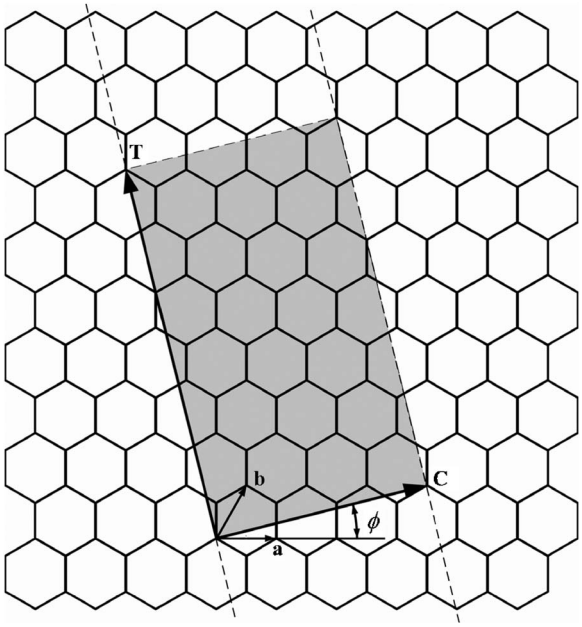

FIG. 20. Schematic illustration of a graphene sheet and definitions of geometrical parameters used to describe a nanotube. A (3, 1) tube would be formed by rolling up the graphene sheet bounded by the two dashed lines. The unit cell of the nanotube is shown in gray.

If the head of a vector **C** in graphene plane touches its tail when the graphene sheet rolled into a tube, we call **C** the chiral vector, or roll-up vector (see Fig. 20). Because a vector **C** in the graphene plane can be described as a combination of two base vectors **a** and **b** of the hexagon by $\mathbf{C}=n\mathbf{a}+m\mathbf{b}$, with n and m being two integers, a SWCNT can be uniquely indexed by a pair of integers (n,m) to represent its chirality or helicity.[75] The magnitude of the chiral vector, $C=\sqrt{3}r_0\sqrt{m^2+n^2+mn}$, represents the circumference of the nanotube, where $r_0=0.142$ nm is the carbon-carbon bond length. The tube radius, R, can thus be calculated by $R=C/2\pi$. The chiral angle ϕ of a nanotube is given by $\phi=\arccos[(2n+m)/(2\sqrt{m^2+n^2+mn})]$. The two limiting cases of nanotubes are $(n,0)$ (whose chiral angle is 0) and (n,n) (whose chiral angle is $\pi/6$), which are usually known as zigzag and armchair tubes based on the geometry of carbon bonds around the circumference of the nanotube. Zigzag and armchair tubes are achiral nanotubes because of the highly geometrical symmetry, whereas SWCNTs with a chiral angle of $0<\phi<\pi/6$ are chiral nanotubes. Another important geometrical parameter of SWCNTs is the translation vector **T**, which is directed along the SWCNT axis and perpendicular to the chiral vector **C** (see Fig. 20). The magnitude of the translation vector, $T=3r_0\sqrt{m^2+n^2+mn}/d_R$ [with $d_R=\gcd(2n+m,2m+n)$], corresponds to the length of the SWCNT unit cell (which is marked in gray in Fig. 20).

We consider a (n,m) SWCNT subjected to an axial force F, a radial pressure P, and an axial torque M_T, as shown in Fig. 21(a). The nonlinear stick-spiral model can then be established by introducing Eqs. (5) and (6) into the linear stick-spiral model.[67]

The equilibriums of the external forces and the internal forces yield

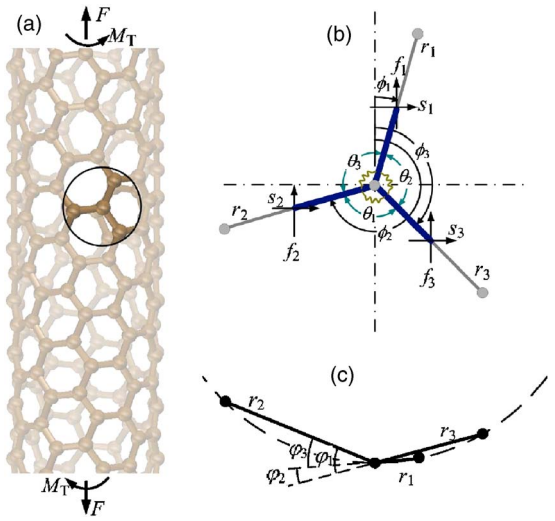

FIG. 21. (Color online) (a) Global structure of a chiral nanotube. (b) Front view of local structure and schematic of the stick-spiral model. In the model, a stick with infinite bending stiffness is used to model force-stretch relationship of the carbon-carbon bond, and a spiral spring is used to describe the twisting moment resulting from an angular distortion of the bond angle. (c) Top view of local structure.

$$F=(n+m)f_1+mf_2, \tag{A1}$$

$$P=-[(n-m)s_1+(2n+m)s_2]/(TR), \tag{A2}$$

$$M_T=[(n+m)s_1+ms_2]R, \tag{A3}$$

where R is the tube radius, and f_i and s_i are forces contributed on carbon bond along axial and circumferential directions, respectively [see Fig. 21(b)].

Equilibrium of the local structure of the SWCNT needs

$$f_1+f_2+f_3=0, \tag{A4}$$

$$s_1+s_2+s_3=0. \tag{A5}$$

Force equilibrium to bond extension leads to

$$f_i\cos\phi_i+s_i\sin\phi_i=F^*(\Delta r_i) \quad i=1,2,3. \tag{A6}$$

From the moment equilibrium of a bond, we obtain

$$\frac{r_i}{2}(f_i\sin\phi_i-s_i\cos\phi_i)=M^*(\Delta\theta_j)\cos\omega_{ij} + M^*(\Delta\theta_k)\cos\omega_{ik} \quad i,j,k = 1,2,3; \quad i\neq j\neq k, \tag{A7}$$

where ω_{ij}, the torsion angle between the plane though r_i parallel to the nanotube axis and the plane of θ_j, can be calculated by

$$\cos\omega_{ij}=(\cos\phi_i\sin\phi_k\cos\varphi_j-\sin\phi_i\cos\phi_k)/\sin\theta_j \quad i,j,k = 1,2,3; \quad i\neq j\neq k. \tag{A8}$$

The structural parameters φ_i, ϕ_I, and θ_i are defined in Figs. 21(b) and 21(c).

The geometrical relationships of a SWCNT satisfy

$$\cos\theta_i = \sin\phi_j \sin\phi_k \cos\varphi_i + \cos\phi_j \cos\phi_k \quad i,j,k = 1,2,3; \quad i \neq j \neq k. \tag{A9}$$

With use of Eqs. (A8) and (A9), the variation of bond angle can be obtained as

$$\Delta\theta_i = -(\Delta\phi_j \cos\omega_{ji} + \Delta\phi_k \cos\omega_{ki}) \quad i,j,k = 1,2,3; \quad i \neq j \neq k. \tag{A10}$$

Cylindrical structure of a defect-free SWCNT always needs its chiral vector to keep a closed ring, i.e., the dislocation between the head and the tail of the chiral vector should be zero no matter how the SWCNT was deformed unless the presence of defects. This feature actually gives a compatible equation of a deformed SWCNT as follows

$$\Delta[mr_1 \cos\phi_1 - (n+m)r_2 \cos\phi_2 + nr_3 \cos\phi_3] = 0. \tag{A11}$$

We now have 15 independent equations given by Eqs. (A1)–(A7), (A10), and (A11), and 18 independent variables F, P, M_T, f_1, f_2, f_3, s_1, s_2, s_3, Δr_1, Δr_2, Δr_3, $\Delta\theta_1$, $\Delta\theta_2$, $\Delta\theta_3$, $\Delta\phi_1$, $\Delta\phi_2$, $\Delta\phi_3$. We note here that F, P, and M_T are applied external forces. Once these forces are given, the present problem is solvable. For example, letting $P=0$ and $M_T=0$, with a stepwise increase in the axial strain ε, the mechanical behavior of a SWCNT under axial loading can be obtained via the non-linear stick-spiral model.

APPENDIX B

In this paper, a SWCNT is treated as a cylindrical shell (with a constant effective thickness t) other than a solid rod. Thus the axial, circumferential, and shear stresses (σ, σ', and τ) and strains (ε, ε', and γ) can be defined as, respectively

$$\sigma = \frac{F}{Ct} = \frac{(n+m)f_1 + mf_2}{\sqrt{3}r_0 t\sqrt{n^2+mn+m^2}}, \tag{B1}$$

$$\sigma' = \frac{PR}{t} = -\frac{(n-m)s_1 + (2n+m)s_2}{3r_0 t\sqrt{n^2+mn+m^2}}, \tag{B2}$$

$$\tau = \frac{M_T}{RCt} = \frac{(n+m)s_1 + ms_2}{\sqrt{3}r_0 t\sqrt{n^2+mn+m^2}}, \tag{B3}$$

$$\varepsilon = \frac{\Delta T}{T} = \frac{d[(2n+m)r_1 \cos\phi_1 - (n-m)r_2 \cos\phi_2 - (2m+n)r_3 \cos\phi_3)]}{3r_0\sqrt{n^2+mn+m^2}}, \tag{B4}$$

$$\varepsilon' = \frac{\Delta C}{C} = \frac{d[mr_1 \sin\phi_1 - (n+m)r_2 \sin\phi_2 + nr_3 \sin\phi_3]}{\sqrt{3}r_0\sqrt{n^2+mn+m^2}}, \tag{B5}$$

$$\gamma = \frac{\Delta[(2n+m)r_1 \sin\phi_1 - (n-m)r_2 \sin\phi_2 - (2m+n)r_3 \sin\phi_3)]}{3r_0\sqrt{n^2+mn+m^2}}. \tag{B6}$$

It should be noted that different values for the effective thickness t of a SWCNT have been obtained in the literatures according to different physical requirements, ranging from 0.066 nm to 0.69 nm, with maximum deviations up to 10 times.[63] Different values for effective tube thickness will obviously affect the quantities of some mechanical parameters, such as the stress and thus the elastic modulus. However, different choices of the value for effective tube thickness have no effect on the qualitative characters of these parameters. Therefore, for the convenience of comparison with the existing results, we simply take the value of effective thickness of a SWCNT as 0.34 nm, as is most commonly used in the literatures.

We note further that the following initial values presented by Chang *et al.*[66,67] for a (n,m) tube have been used in the present calculations

$$r_1 = r_2 = r_3 = r_0, \tag{B7}$$

$$\phi_1 = \arccos\frac{2n+m}{2\sqrt{n^2+mn+m^2}}, \quad \phi_2 = \frac{4\pi}{3} + \phi_1, \quad \phi_3 = \frac{2\pi}{3} + \phi_1, \tag{B8}$$

$$\varphi_1 = \frac{\pi}{\sqrt{n^2+mn+m^2}}\cos\phi_1, \quad \varphi_2 = \frac{\pi}{\sqrt{n^2+mn+m^2}}\cos\left(\frac{\pi}{3} + \phi_1\right), \quad \varphi_2 = \frac{\pi}{\sqrt{n^2+mn+m^2}}\cos\left(\frac{\pi}{3} - \phi_1\right). \tag{B9}$$

*Corresponding author. Email address: tchang@staff.shu.edu.cn

[1] R. E. Smalley and B. I. Yakobson, Solid State Commun. **107**, 597 (1998).
[2] R. H. Baughman, A. A. Zakhidov, and W. A. de Heer, Science **297**, 787 (2002).
[3] A. N. Guz and Y. Y. Rushchitskii, Int. Appl. Mech. **39**, 1271 (2003).
[4] M. M. J. Treacy, T. W. Ebbesen, and J. M. Gibson, Nature (London) **381**, 680 (1996).
[5] A. Krishnan, E. Dujardin, T. W. Ebbesen, P. N. Yianilos, and M. M. J. Treacy, Phys. Rev. B **58**, 14013 (1998).
[6] P. Poncharal, Z. L. Wang, D. Ugarte, and W. A. de Heer, Science **283**, 1513 (1999).
[7] E. W. Wong, P. E. Sheehan, and C. M. Lieber, Science **277**, 1971 (1997).
[8] J. P. Salvetat, A. J. Kulik, J. M. Bonard, G. A. D. Briggs, T. Stockli, K. Metenier, S. Bonnamy, F. Beguin, N. A. Burnham, and L. Forro, Adv. Mater. (Weinheim, Ger.) **11**, 161 (1999).
[9] M. F. Yu, O. Lourie, M. J. Dyer, K. Moloni, T. F. Kelly, and R. S. Ruoff, Science **287**, 63 (2000).
[10] B. G. Demczyk, Y. M. Wang, J. Cumings, M. Hetman, W. Han, A. Zettl, and R. O. Ritchie, Mater. Sci. Eng., A **334**, 173 (2002).
[11] D. H. Robertson, D. W. Brenner, and J. W. Mintmire, Phys. Rev. B **45**, 12592 (1992).
[12] E. Hernandez, C. Goze, P. Bernier, and A. Rubio, Phys. Rev. Lett. **80**, 4502 (1998).
[13] D. Sanchez-Portal, E. Artacho, J. M. Soler, A. Rubio, and P. Ordejon, Phys. Rev. B **59**, 12678 (1999).
[14] V. N. Popov, V. E. Van Doren, and M. Balkanski, Phys. Rev. B **61**, 3078 (2000).
[15] B. I. Yakobson, C. J. Brabec, and J. Bernholc, Phys. Rev. Lett. **76**, 2511 (1996).
[16] A. Garg, J. Han, and S. B. Sinnott, Phys. Rev. Lett. **81**, 2260 (1998).
[17] R. C. Krenn, D. Roundy, M. L. Cohen, D. C. Chrzan, and J. W. Morris, Phys. Rev. B **65**, 134111 (2002).
[18] Y. N. Gartstein, A. A. Zakhidov, and R. H. Baughman, Phys. Rev. B **68**, 115415 (2003).
[19] Y. Wang, X. X. Wang, and X. G. Ni, Modell. Simul. Mater. Sci. Eng. **12**, 1099 (2004).
[20] K. M. Liew, C. H. Wong, X. Q. He, M. J. Tan, and S. A. Meguid, Phys. Rev. B **69**, 115429 (2004).
[21] L. F. Wang, Q. S. Zheng, J. Z. Liu, and Q. Jiang, Phys. Rev. Lett. **95**, 105501 (2005).
[22] C. L. Zhang and H. S. Shen, Carbon **44**, 2608 (2006).
[23] X. Chen and G. Cao, Nanotechnology **17**, 1004 (2006).
[24] H. Y. Liang and M. Upmanyu, Phys. Rev. Lett. **96**, 165501 (2006).
[25] T. Chang, J. Hou, and X. Guo, Appl. Phys. Lett. **88**, 211906 (2006).
[26] T. Belytschko, S. P. Xiao, G. C. Schatz, and R. Ruoff, Phys. Rev. B **65**, 235430 (2002).
[27] S. Ogata and Y. Shibutani, Phys. Rev. B **68**, 165409 (2003).
[28] Y. Shibutani and S. Ogata, Modell. Simul. Mater. Sci. Eng. **12**, 599 (2004).
[29] T. Xiao, X. Xu, and K. Liao, J. Appl. Phys. **95**, 8145 (2004).
[30] B. I. Yakobson, M. P. Campbell, C. J. Brabec, and J. Bernholc, Comput. Mater. Sci. **8**, 341 (1997).
[31] M. B. Nardelli, B. I. Yakobson, and J. Bernholc, Phys. Rev. Lett. **81**, 4656 (1998).
[32] M. B. Nardelli, B. I. Yakobson, and J. Bernholc, Phys. Rev. B **57**, R4277 (1998).
[33] M. B. Nardelli, J. L. Fattebert, D. Orlikowski, C. Roland, Q. Zhao, and J. Bernholc, Carbon **38**, 1703 (2000).
[34] Q. Zhao, M. B. Nardelli, and J. Bernholc, Phys. Rev. B **65**, 144105 (2002).
[35] K. M. Liew, X. Q. He, and C. H. Wong, Acta Mater. **52**, 2521 (2004).
[36] K. M. Liew, C. H. Wong, and M. J. Tan, Acta Mater. **54**, 225 (2006).
[37] T. Dumitrica, M. Hua, and B. I. Yakobson, Proc. Natl. Acad. Sci. U.S.A. **103**, 6105 (2006).
[38] P. Zhang, Y. Huang, P. H. Geubelle, P. A. Klein, and K. C. Hwang, Int. J. Solids Struct. **39**, 3893 (2002).
[39] M. Arroyo and T. Belytschko, Phys. Rev. Lett. **91**, 215505 (2003).
[40] D. Qian, G. J. Wagner, and W. K. Liu, Comput. Methods Appl. Mech. Eng. **193**, 1603 (2004).
[41] A. Pantano, D. M. Parks, and M. C. Boyce, J. Mech. Phys. Solids **52**, 789 (2004).
[42] H. W. Zhang, J. B. Wang, and X. Guo, J. Mech. Phys. Solids **53**, 1929 (2005).
[43] X. Guo, J. B. Wang, and H. W. Zhang, Int. J. Solids Struct. **43**, 1276 (2006).
[44] G. Cao and X. Chen, Phys. Rev. B **73**, 155435 (2006).
[45] T. S. Gates, G. M. Odegard, S. J. V. Frankland, and T. C. Clancy, Compos. Sci. Technol. **65**, 2416 (2005).
[46] M. Wang, X. Zhang, and M. W. Lu, Phys. Rev. B **72**, 205403 (2005).
[47] A. Y. T. Leung, X. Guo, X. Q. He, H. Jiang, and Y. Huang, J. Appl. Phys. **99**, 124308 (2006).
[48] M. Meo and M. Rossi, Compos. Sci. Technol. **66**, 1597 (2006).
[49] C. W. S. To, Finite Elem. Anal. Design **42**, 404 (2006).
[50] C. Q. Ru, Phys. Rev. B **62**, 16962 (2000).
[51] C. Y. Wang, C. Q. Ru, and A. Mioduchowski, Int. J. Solids Struct. **40**, 3893 (2003).
[52] S. Kitipornchai, X. Q. He, and K. M. Liew, Phys. Rev. B **72**, 075443 (2005).
[53] M. J. Longhurst and N. Quirke, J. Chem. Phys. **124**, 234708 (2006).
[54] H. S. Shen, Int. J. Solids Struct. **41**, 2643 (2004).
[55] X. Wang and H. K. Yang, Phys. Rev. B **73**, 085409 (2006).
[56] H. S. Shen and C. L. Zhang, Phys. Rev. B **74**, 035410 (2006).
[57] Q. Wang, V. K. Varadan, and S. T. Quek, Phys. Lett. **357**, 130 (2006).
[58] Y. Q. Zhang, G. R. Liu, and X. Han, Phys. Lett. **349**, 370 (2006).
[59] C. Y. Wang, C. Q. Ru, and A. Mioduchowski, ASME J. Appl. Mech. **71**, 622 (2004).
[60] G. M. Odegard, T. S. Gates, L. M. Nicholson, and K. E. Wise, Compos. Sci. Technol. **62**, 1869 (2002).
[61] G. M. Odegard, T. S. Gates, L. M. Nicholson, and K. E. Wise, Report No. NASA/TM-2002–211454 (2002).
[62] Q. Wang, Int. J. Solids Struct. **41**, 5451 (2004).
[63] T. Chang and H. Gao, J. Mech. Phys. Solids **51**, 1059 (2003).
[64] L. Shen and J. Li, Phys. Rev. B **69**, 045414 (2004).
[65] A. Y. T. Leung, X. Guo, X. Q. He, and S. Kitipornchai, Appl. Phys. Lett. **86**, 083110 (2005).
[66] T. Chang, J. Geng, and X. Guo, Appl. Phys. Lett. **87**, 251929 (2005).

[67] T. Chang, J. Geng, and X. Guo, Proc. R. Soc. London, Ser. A **462**, 2523 (2006).
[68] T. Chang, W. Guo, and X. Guo, Phys. Rev. B **72**, 064101 (2005).
[69] T. Chang, G. Li, and X. Guo, Carbon **43**, 287 (2005).
[70] J. R. Xiao, B. A. Gama, and J. W. Gillespie, Int. J. Solids Struct. **42**, 3075 (2005).
[71] J. R. Xiao and J. W. Gillespie, Phys. Rev. B **74**, 155404 (2006).
[72] D. A. Walters, L. M. Ericson, and M. J. Casavant, Appl. Phys. Lett. **74**(25), 3803 (1999).
[73] E. Ertekin and D. C. Chrzan, Phys. Rev. B **72**, 045425 (2005).
[74] S. Gupta, K. Dharamvir, and V. K. Jindal, Phys. Rev. B **72**, 165428 (2005).
[75] C. T. White, D. H. Robertson, and J. W. Mintmire, Phys. Rev. B **47**, 5485 (1993).